Real-Time Observation of a Coherent Lattice Transformation into a High-Symmetry Phase

Samuel W. Teitelbaum,[1,*] Taeho Shin,[2,†] Johanna W. Wolfson,[1] Yu-Hsiang Cheng,[3] Ilana J. P. Molesky,[1]
Maria Kandyla,[4,1] and Keith A. Nelson[1,‡]

[1]*Department of Chemistry, Massachusetts Institute of Technology, Cambridge, Massachusetts 02139, USA*
[2]*Department of Chemistry, Chonbuk National University, Jeonju 54896, Republic of Korea*
[3]*Department of Electrical Engineering and Computer Science, Massachusetts Institute of Technology,
Cambridge, Massachusetts 02139, USA*
[4]*Theoretical and Physical Chemistry Institute,
National Hellenic Research Foundation, Athens 11635, Greece*

Excursions far from their equilibrium structures can bring crystalline solids through collective transformations including transitions into new phases that may be transient or long-lived. The direct spectroscopic observation of far-from-equilibrium rearrangements provides fundamental mechanistic insight into chemical and structural transformations and a potential route to practical applications, including ultrafast optical control over material structure and properties. However, in many cases, photoinduced transitions are irreversible or only slowly reversible, or the light fluence required exceeds material damage thresholds. This requirement precludes conventional ultrafast spectroscopy, in which optical excitation and probe pulses irradiate the sample many times, each measurement providing information about the sample response at just one probe delay time following excitation, with each measurement at a high repetition rate and with the sample fully recovering its initial state in between measurements. Using a single-shot, real-time measurement method, we are able to observe the photo-induced phase transition from the semimetallic, low-symmetry phase of crystalline bismuth into a high-symmetry phase whose existence at high electronic excitation densities is predicted based on earlier measurements at moderate excitation densities below the damage threshold. Our observations indicate that coherent lattice vibrational motion launched upon photoexcitation with an incident fluence above 10 mJ/cm^2 in bulk bismuth brings the lattice structure directly into the high-symmetry configuration for several picoseconds, after which carrier relaxation and diffusion restore the equilibrium lattice configuration.

Subject Areas: Condensed Matter Physics,
Materials Science,
Physical Chemistry

I. INTRODUCTION

Crystals with symmetry-lowering Peierls distortions [1–5] present particularly attractive targets for time-resolved measurements of collective transitions to new structural phases. Like their molecular counterparts with Jahn-Teller distortions, Peierls-distorted systems arise due to coupling between electrons in partially filled states of nearby energy and vibrational modes along whose

[*]samuelt@mit.edu
[†]shin@jbnu.ac.kr
[‡]kanelson@mit.edu

coordinates the distortions occur. The energy cost of the vibrational excursion is more than compensated for by the associated splitting of degenerate or near-degenerate electronic states, with electrons populating the lower-energy states. Optical excitation removes electrons from those states, reducing the energy payback for vibrational distortion. Under sufficiently intense illumination, the distortion might be removed completely.

The semimetal bismuth is a prototypical Peierls system [6], where its rhombohedral crystal lattice is related to a simple cubic structure (observed in antimony at elevated pressures as the stable, metallic phase [7,8]) through the motion of atoms away from the high-symmetry locations along the unit-cell diagonals, corresponding to the A_{1g} optic phonon mode of the rhombohedral phase. This collective distortion opens a band gap to produce the semimetallic phase. Previous ultrafast spectroscopic studies on bismuth have shown time-dependent oscillations of the A_{1g} phonon
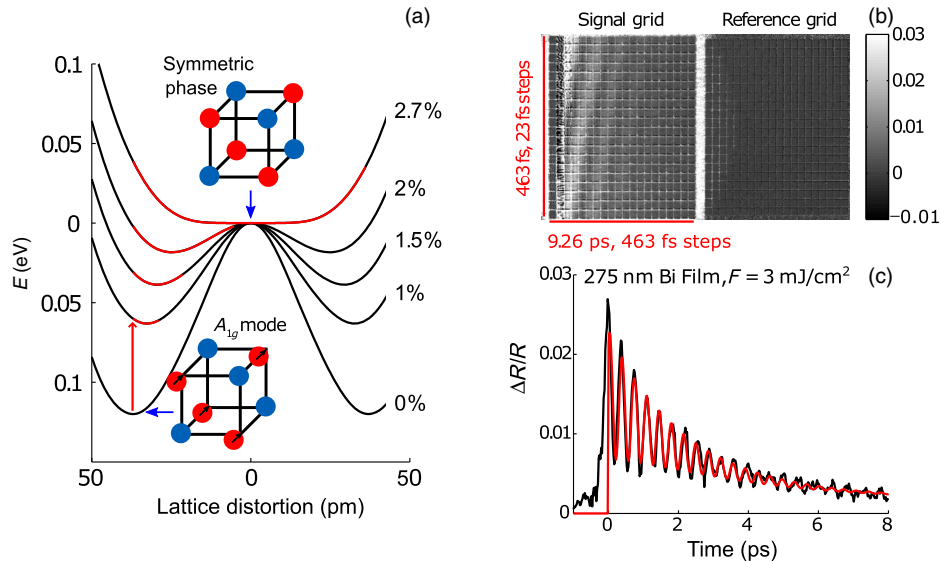
FIG. 1. Dual-echelon single-shot spectroscopy of bismuth. (a) Potential energy surface of bismuth along the A_{1g} mode coordinate at various levels of electronic excitation. The range of coherent lattice motion upon fast excitation from the ground state is shown in red along the curves. At excitation densities above 2% of the valence electrons, the kinetic energy imparted to the A_{1g} mode is enough to drive the central atom (shown in red in the schematic) across the center of the unit cell, forming the symmetric phase. The distorted (bottom) and symmetric (top) crystal structures are shown in (a), with arrows showing the direction of motion of the central atom (red). The lattice distortion is exaggerated for clarity. (b) Differential image of the echelon grid on a 275-nm-thick bismuth film, excited with a fluence of 3 mJ/cm² and a probe wavelength of 800 nm, on a scale of −1% to 3% $\Delta R/R$, showing coherent phonon oscillations on the signal (left) grid. This image is averaged over 50 laser shots. (c) Unfolded single-shot pump-probe trace extracted from the image in (b), showing coherent phonon oscillations of the A_{1g} mode. The red curve shows the fit to Eqs. (1) and (2).

mode, with significant softening of the phonon frequency as the excitation density is increased up to 1.5% of the valence electrons [4]. Density-functional-theory (DFT) calculations by Murray *et al.* [3] predict that, if the electronic excitation is strong enough (>2% of valence electrons excited), it should be possible to drive the bismuth atom past the center of the unit cell and reach a transient high-symmetry structure, shown in Fig. 1(a). This photo-induced phase transition, which has not yet been observed, is predicted to be nonthermal, and the high-symmetry phase cannot be reached by raising the temperature. The lattice change occurs due to exceptionally strong electron-phonon coupling, as the removal of valence electrons upon optical absorption changes the lattice potential preceding any loss of electron energy to the lattice. In contrast, in aluminum and many other metals, carrier excitation has a minimal effect on the lattice potential energy, and phase transitions such as lattice melting proceed through the transfer of energy from hot carriers to the initially cold lattice over a few picoseconds [9].

The removal of a lattice distortion by electronic excitation has been observed in other systems with Peierls-like distortions, such as VO_2 [10], blue bronze [5], charge-ordered manganites [11–13], organic crystals [1,2], and rare-earth chalcogenides [5,14], and predicted theoretically in arsenic and antimony [15,16]. Despite bismuth's status as a canonical Peierls system, sample damage at high excitation densities has prevented the observation of electronic lifting

of the Peierls distortion analogous to what has been observed in these systems, and its low melting point prevents the observation of the high-symmetry phase at thermal equilibrium. The experimental observation of electronic lifting of the Peierls distortion in bismuth provides a benchmark for electronic lifting of a Peierls distortion in a relatively well-understood system with minimal electron correlation, where the observed dynamics are purely structural.

Previously, Fritz *et al.* performed optical pump x-ray probe measurements in bismuth, showing bond softening and an approach toward the symmetric phase [4]. However, sample damage prevented exploration at excitation densities beyond where 1.3% of the valence electrons are excited. Sciaini *et al.* probe photoexcited bismuth with femtosecond electron diffraction and show evidence of nonthermal melting faster than 1 ps after high-fluence excitation above the damage threshold [17], and Sokolowski-Tinten *et al.* report x-ray diffraction measurements that show a partial loss of long-range order after several picoseconds [18].

The results to date leave open the question of whether a transient high-symmetry crystalline state in bismuth may be reached upon photoexcitation. In this hidden phase, the unit cell would be halved in size, with only one atom per unit cell and no optic phonon modes. Therefore, the absence of coherent optical phonon oscillations in a time-resolved pump-probe trace with a high pump fluence could indicate a higher-symmetry crystalline phase with no long-range order between bismuth dimers. However, the Raman-active

A_{1g} optic phonon mode is also absent in liquid and amorphous solid systems. Lowering the initial sample temperature precludes thermal melting at a high laser fluence. The time-dependent reflectivity can then monitor the time-dependent evolution of the lattice distortion closely, but such data are difficult to collect if each high-fluence excitation laser shot is followed by a single probe pulse that records the transient optical properties at a single delay time. In that case, permanent damage of each irradiated sample region allows data to be recorded only at a few time delays, with a limited signal-to-noise ratio because extensive signal averaging is impossible and the time dependence must be determined by combining measurements at different delays from different sample regions. Here, we report results of measurements that circumvent these limitations by recording the sample response at many delay times after each excitation pulse [19], providing an experimental probe of a hidden solid phase and the measurement of the dynamics of its formation and relaxation.

II. METHODS

The bismuth samples are polycrystalline thin films sputtered on sapphire and glass substrates, with film thicknesses of 20 and 275 nm (essentially bulk). See Supplemental Material [20] for more details on the sample characterization (Figs. S1–S3). The substrates are heated to 170 °C during sputter coating to ensure crystalline deposition. Substrates are sonicated in acetone to remove any residual surface deposits and then plasma cleaned in the sputter coater before deposition. Powder diffraction confirms the samples are crystalline and slightly textured with the surface preferentially oriented along the (1 1 1) direction, as shown in Supplemental Material [20] (Fig. S3).

Single-shot transient-reflection pump-probe measurements are conducted using a method demonstrated earlier [19] in which a 20 × 20 grid of 400 probe pulses is focused onto the same region of the sample as an 800-nm excitation pulse, with the probe pulse time delays incremented by 23 fs. The reflected probe pulses are projected onto a CCD camera, where they again form a 20 × 20 grid, allowing the data from each of the 400 time delays to be read out. The method is summarized in Supplemental Material [20] (Sec. II, Fig. S5), and representative images and traces are shown in Figs. 1(b) and 1(c), respectively.

To ensure that melting could not occur before the formation of the symmetric phase, the experiments are performed with an initial sample temperature of 80 K, well below bismuth's melting point of 544 K. Depending on the pump fluence, 20–100 shots are recorded from each sample region before permanent damage occurs, as assessed by changes in the static reflectivity and by pump-probe time-dependent signals that are recorded at a low fluence, and confirmed after the experiment by checking for visible damage on the sample surface with an optical microscope (see Supplemental Material [20], Fig. S7, for more details).

The pump spot size is approximately 1 mm in diameter on the sample and is determined by placing a camera at the sample position.

III. RESULTS

A. Single-shot spectroscopy

Single-shot data from the bulklike (275-nm film) and thin-film (20-nm film) samples are shown in Fig. 2. Reflectivity traces for the bulk sample are shown in Figs. 2(a) and 2(b), while similar traces for the 20-nm thin film are shown in Fig. S6 in Supplemental Material [20]. In bulk bismuth, upon increasing the excitation fluence, the lifetime of the coherent phonon mode drops dramatically, and the frequency drops from its equilibrium value of 2.95 THz down to a minimum measurable value of 1.8 THz [Fig. 2(c), solid circles]. Above 9 mJ/cm^2, the coherent phonon oscillations persist for less than a half cycle [Fig. 2(b)], indicating that the coherent lattice vibrational motion initiated upon photoexcitation through electron-phonon coupling propels the atoms directly into their positions in the high-symmetry phase. Above this fluence, the initial potential energy along the vibrational coordinate in the excited state is higher than the barrier in the center of the unit cell, as shown in Fig. 1(a). The initial motion of the bismuth atoms toward (and past) the center of the unit cell, followed by rapid dephasing, randomizes the Bi atom positions in their local potential minima about the unit-cell centers, thereby forming the high-symmetry phase.

We see similar results in bond softening and the eventual disappearance of coherent oscillations at 300 and 80 K in both the 20- and 275-nm thin films. In the 20-nm film, lower pump fluences are required for similar reductions in the phonon frequency and for the disappearance of the phonon oscillations [Fig. 2(c), empty circles]. As discussed earlier [22], the confinement of excited carriers in the thin film preserves a higher carrier density than in the thicker sample, in which fast carrier diffusion quickly reduces the photo-excited electron density. This confinement accounts for more pronounced thin-film responses at lower pump fluences, as noted in several studies [4,18,22]. Quantum confinement and backreflections from the substrate in the 20-nm thin film reverse the sign of the reflectivity change and reduce the amplitudes of the reflectivity oscillations compared to the bulk sample [22] but do not affect the excitation density dependence of the lattice potential. The fluence-dependent trend in bond softening does not change significantly with a sample temperature between 300 and 80 K [Fig. 2(c)]. Small differences may be due to thermal contraction and a slightly higher carrier diffusivity at a low temperature.

To measure coherent phonon frequencies in double-pump and single-pump pump-probe experiments, single-shot traces are fit to a decaying background signal of the form

$$\left(\frac{\Delta R}{R}\right)_{bgd} = A_1 e^{-t/\tau_{el}} + A_2, \tag{1}$$
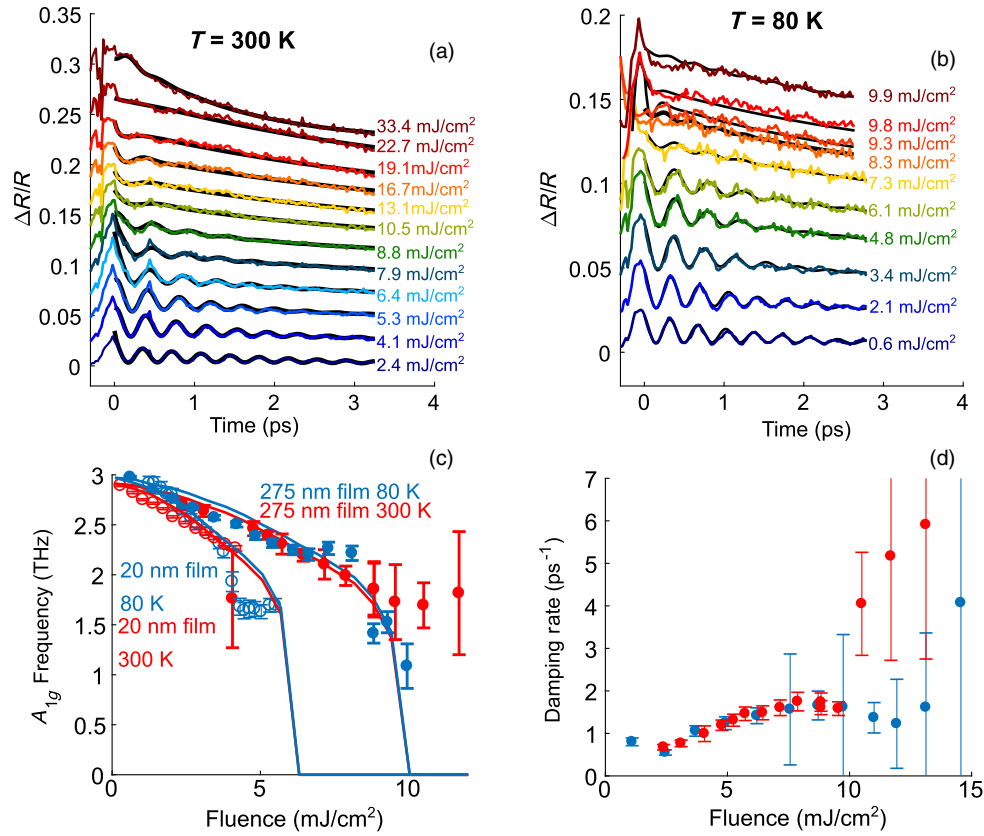
FIG. 2. (a) Single-shot pump-probe traces for 275-nm Bi films with an initial temperature of 300 K. (b) Single-shot pump-probe traces for 275-nm Bi films with an initial temperature of 80 K. In (a) and (b), the colored lines are experimental data, and the black curves are fits of the experimental data to Eqs. (1) and (2), as described in the text. (c) The coherent phonon frequency at 300 and 80 K as a function of the fluence for two separate films: one 20 nm thick and one 275 nm thick. Lines are simulation curves calculated using the photoexcited carrier density from an extended two-temperature model [21] and the carrier density-dependent anharmonic lattice potential [3]. At high fluences, the fitting used to calculate a damping rate breaks down when the coherent phonons vanish (above 10.5 mJ/cm² in the 275-nm film at 300 K and above 9 mJ/cm² at 80 K). The probe wavelength for all traces in this figure is 800 nm, and traces are offset for clarity. (d) The damping rate of the coherent oscillations, which increases with photoexcitation fluence.

where τ_{el} is the decay time of the slowly varying background and A_1 and A_2 are the amplitudes of the decaying and quasi-dc components. To obtain the phonon frequency, the trace is subtracted from the fitted background and fit to a decaying sine function of the form

$$\left(\frac{\Delta R}{R}\right)_{osc} = A\cos(2\pi ft)e^{-\gamma t}, \tag{2}$$

where f is the coherent A_{1g} phonon frequency, A is the amplitude of the phonon oscillation, and γ is the phonon damping rate. The chirp in the A_{1g} mode oscillation observed in previous studies [3,23,24] is not necessary for fitting traces under a very high fluence excitation and most two-pulse data after high fluence excitation, because the oscillation lifetime is sufficiently short that no change in the oscillation frequency is measurable during the decay time. Fits (black lines) are shown superimposed on the raw data (color) for each single-shot trace as a function of the fluence in Figs. 2(a) and 2(b). The fitted frequency f and damping rate γ as a

function of the fluence are shown in Figs. 2(c) and 2(d), respectively. The fitting breaks down at a high fluence when the coherent oscillation is seen for less than a half cycle, very close to and above the onset of the symmetric phase.

As discussed below, thermal modeling shows that an excitation fluence of 20 mJ/cm² or below is not sufficient to bring the surface of the 275-nm sample from 80 K to the melting point, indicating that the loss of the phonon signal is due to a transition into the high-symmetry crystalline phase rather than melting. To probe the structural evolution of the bismuth crystal after strong photoexcitation, we irradiate the sample with a second, weak excitation pulse at various time delays following the first strong pump pulse, and we measure the time-dependent signal following the second pulse. This measurement allows us to observe the recovery of phonon oscillations induced by a weak pump pulse, indicating if the crystal had returned to the low-symmetry phase by the time that the second pulse arrived [10]. Figure 3(a) shows results from the 275-nm film at 80 K for a first pump fluence of 10.9 mJ/cm² and a second
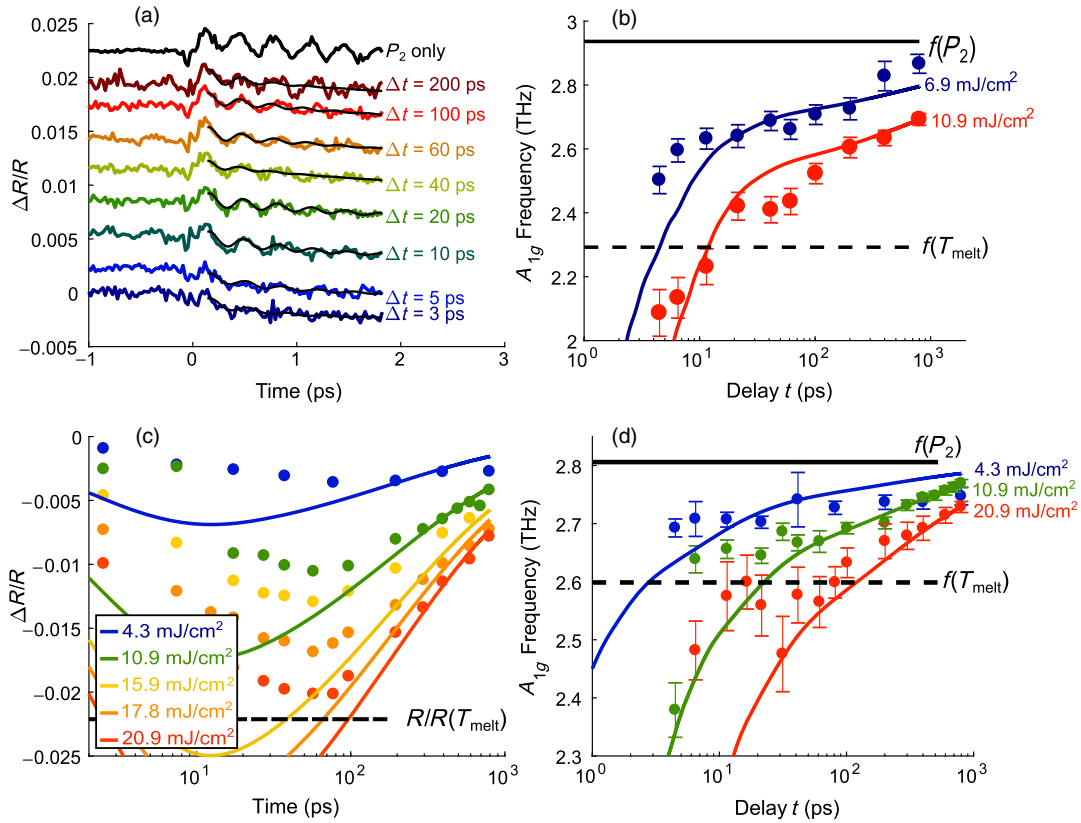
FIG. 3. Two-pulse experiments on the highly excited state of the 275-nm bismuth film. (a) Single-shot traces following an initial excitation pulse (P_1) of 10.9 mJ/cm² and a second excitation pulse (P_2) of 1 mJ/cm² on a 275-nm film at 80 K. The coherent phonon signal is suppressed 3 ps after the first excitation pulse and returns 20 ps later. Δt is the time delay between the two excitation pulses. The probe wavelength for this experiment is 720 nm. (b) Coherent phonon frequency as a function of the time delay between an initial excitation pulse with an incident fluence of 6.9 and 10.9 mJ/cm² and a second excitation pulse with an incident fluence of $P_2 = 1$ mJ/cm². The solid lines are the predicted oscillation frequency based on an extended two-temperature model. Within 1 ps after excitation at 10.9 mJ/cm², no phonon oscillations are induced by a weak second excitation pulse, indicating that the irradiated region of the film is in the symmetric phase. (c) The transient reflectivity of the Bi film at 300 K as a function of time after excitation for various pump fluences with an 800-nm probe. Note the logarithmic timescale. Points are measurements made at selected long times averaged over the 9-ps time window of the single-shot instrument. Solid lines are calculations based on an extended two-temperature model and the known thermoreflectance of bismuth. The simulations do not account for the reflectivity change due to hot carriers, and so are expected to agree only with the experiment at a long delay. The dashed line labeled $\Delta R/R(T_{melt})$ corresponds to the relative reflectivity difference of bismuth at its initial temperature of 300 K and its melting point $T_{melt} = 544$ K. (d) Transient A_{1g} frequency measured using the same method as in (b) for the sample starting at 300 K for three representative pump fluences. The solid line labeled $f(P_2)$ corresponds to the coherent phonon frequency observed by the weak pump pulse in the absence of the strong pump P_1. The dashed line indicates the expected A_{1g} phonon frequency for bismuth heated to its melting point.

pump fluence of 1 mJ/cm². After a delay of 3 ps between the first and the second pump pulses, there is no indication of coherent oscillations induced by the second pulse. After a 20-ps delay between the first and second pump pulses, the coherent oscillations are clearly present. For the initial pump fluence of 10.9 mJ/cm², the phonon oscillations return within 10 ps. The oscillation frequency as a function of the delay of the second pump pulse with respect to the first pump pulse, for two fluence values of the first pump pulse, is shown in Fig. 3(b). The low first pump pulse fluence of 7 mJ/cm² is below the transition threshold to the symmetric phase, and the higher pump pulse fluence of 10 mJ/cm² is above the transition

threshold. The picosecond timescale for restoration of the low-symmetry crystalline state is consistent with the kinetics of electron-hole recombination and diffusion but is clearly inconsistent with recrystallization from a liquid state through either nucleation or growth from nearby crystalline regions, which would be on the order of nanoseconds or more. The picosecond timescale indicates that the disappearance of the Peierls distortion as measured by the absence of an A_{1g} coherent phonon is not due to the formation of a liquid phase through either thermal or nonthermal melting. The results of a two-pump experiment on the same film with an initial sample temperature of 300 K are shown in Fig. 3(d), showing a similar

recovery timescale of the coherent phonon frequency. The symmetric phase is reached for the trace with an initial pump fluence of 10.9 mJ/cm^2.

Furthermore, the single-shot instrument permits us to measure the time-dependent reflectivity after the initial, strong excitation pulse for up to 1 ns following photo-excitation. The final time-dependent reflectivity change can be used as a secondary check of the final lattice temperature after a strong photoexcitation pulse, using the known thermoreflectance of bismuth. The time-dependent reflectivities at 800 nm at various pump fluences are shown in Fig. 3(c). For a probe wavelength of 800 nm, the thermoreflectance parameter in bismuth is $dR/dT = -9 \times 10^{-5}$ K^{-1} [25]. Therefore, the 4% change in reflectivity after excitation with a 20 mJ/cm^2 pulse corresponds to a 500-K temperature jump. This result is in good agreement with our thermal model at later time delays (> 60 ps) as discussed in the next section.

B. Modeling and simulations

We can calculate the expected carrier density within the optical penetration depth based on the excitation fluence and the carrier diffusion rate. Then, we can use the potential energy surface calculated by Murray *et al.* [3] to relate the carrier density at the irradiated sample surface to the phonon frequency. Based on our calculations for carrier diffusion and the measured phonon frequency, the maximum photoexcited carrier density reached at the surface in the experiments presented here is greater than 2% of the valence electrons excited, which is above the calculated threshold for the structural phase transition in bulk Bi. The photoexcitation of 2% valence electrons threshold is reached with a pump fluence of 9.2 mJ/cm^2.

Using an extended two-temperature model [19], we simulate carrier diffusion and thermalization away from the irradiated sample surface and thermalization with the lattice as a function of time t and depth z, the results of which are shown in Fig. 4. The extended two-temperature model is the solution to the coupled equations for the carrier density, carrier temperature, and lattice temperature. The excited carrier density n_e is described by the diffusion equation

$$\frac{\partial n_e}{\partial t} = D_e \frac{\partial^2 n_e}{\partial z^2} - \frac{1}{\tau}[n_e - n_0(T_l)]. \quad (3)$$

The parameter D_e is the ambipolar carrier diffusivity, τ is the carrier lifetime, and n_0 is the equilibrium carrier density at lattice temperature T_l. The carriers also have a high nonequilibrium temperature T_e (on the order of a few eV) which evolves in space and time with the modified diffusion equation

$$C_e \frac{\partial T_e}{\partial t} = D_e \frac{\partial^2 T_e}{\partial z^2} - g(T_e)(T_e - T_l). \quad (4)$$
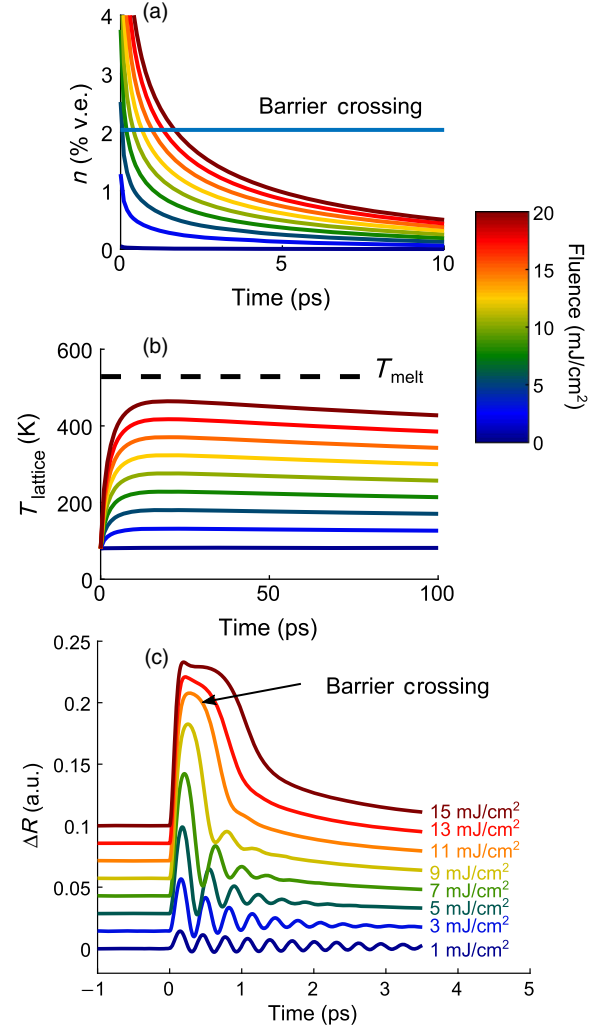

FIG. 4. Extended two-temperature modeling in bismuth. (a) The average carrier density within the optical penetration depth for the first 10 ps after excitation, for a range of fluences comparable to those used in the experiment. The line corresponds to the carrier density required for bismuth atoms to be accelerated over the potential barrier at the center of the unit cell and enter the symmetric phase upon excitation with a short pulse. (b) The lattice temperature in bulk Bi for the first 100 ps after excitation with an initial temperature of 80 K averaged over the penetration depth. The maximum lattice temperature is reached 15 ps after excitation. The dashed line shows the melting temperature of bismuth (544 K). The melting temperature plus heat of fusion required to melt the surface is out of the range of the graph. (c) Simulations of the A_{1g} contribution to the reflectivity obtained by solving the classical equations of motion for the A_{1g} mode on a time-dependent potential defined by the carrier density in (a). The *y*-axis ΔR is the square of the displacement along the A_{1g} mode coordinate x relative to the symmetric position $x = 0$ (in arbitrary units) displaced from its initial position x_0, which is proportional to the change in reflectivity induced by the coherent lattice oscillation, as given by Eq. (7). The simulated trace at 9.2 mJ/cm^2 crosses the barrier at the center of the unit cell, forming the symmetric phase for 1–2 ps, depending on the excitation fluence.

In this equation, C_e is the carrier heat capacity (per carrier), and D_e is the carrier thermal diffusivity. As the carriers cool, the lattice heats equivalently. The heat equation for the lattice temperature T_l is given by

$$C_l \frac{\partial T_l}{\partial t} = D_l \frac{\partial^2 T_l}{\partial z^2} + g_0(T_e - T_l) + \frac{1}{\tau}[E_g + T_e C_e](n_e - n_0),$$
(5)

where C_l is the lattice heat capacity, D_l is the lattice thermal diffusivity, and E_g is the band gap. The first term describes thermal transport into the depth of the material, the second term accounts for heating by carrier-lattice thermalization through electron-phonon coupling, and the third term accounts for lattice heating through hot carrier recombination.

Additional details, equations, and parameters of the extended two-temperature model are given in Supplemental Material [20] and in Ref. [21]. The parameters used for the extended two-temperature model agree well with previous results at a moderate excitation density [4,21,24,26]. Our simulations show the maximum lattice temperature $T_{\max}$ is reached 25 ps after excitation, and 90% of the lattice temperature jump is complete within 5 ps. This lattice temperature rise is consistent with similar results using conventional two-temperature models [26–28], which do not take into account independent carrier density and temperature (see Supplemental Material [20], Fig. S10, for more details). The lattice would reach the melting point T_{melt} with enough excess heat to surpass the heat of fusion in the heated volume only with a far higher fluence than that required to reach the symmetric phase. At 80 K, the surface temperature reaches the melting point at a comparable excitation fluence to the onset of the high-symmetry phase transition but is never heated past the heat of fusion required for melting to occur over the probe penetration depth (15 nm). In order for a liquid phase to form, the bismuth film must be superheated well past the melting point order to overcome the activation energy required to form a solid-liquid interface [29]. Based on our thermal model, $T_{\max}/T_m$ is less than 1.1, which results in melting times well over one second using the homogeneous nucleation theory [29]. A small liquid layer could form near the surface in tens of picoseconds but cannot account for the complete loss of the coherent phonon signal at high excitation densities.

Based on the carrier density and lattice temperature calculated using our transport and thermalization models, we can predict the A_{1g} phonon frequency after excitation and compare with the experimentally determined A_{1g} phonon frequency. The comparison is shown between the points and curves in Fig. 3, which agree to within the uncertainties of our fitting. As the photoexcited carriers recombine, the lattice distortion and coherent phonon frequency recover toward their equilibrium values. The persistence of the

phonon frequency redshift at long times (>60 ps) is due to heating of the bismuth film [23]. The predicted coherent phonon frequencies based on the lattice temperature [Fig. 4(a)] and carrier density [Fig. 4(b)] simulated by an extended two-temperature model agree well with the measured phonon frequencies.

Similarly, we can use the final reflectivity after the strong excitation pulse as a secondary thermometer at long delays, given the known thermoreflectance of bismuth. The time-dependent reflectivity is shown in Fig. 3(c). In comparison with our model, the reflectivity agrees with our model to within 20% at delays longer than 80 ps. Given the accuracy of the thermoreflectance parameter, this agreement is effectively within the margin of error of our model and demonstrates that our thermal model correctly predicts the lattice temperature at late times. At early times, when hot carriers persist and have not thermalized with the lattice, we would not expect the lattice temperature alone to describe the transient reflectivity change of the sample. Nevertheless, the agreement at late times indicates that the thermal model is able to estimate the overall lattice heating 80 ps after the excitation pulse. The expected time for minimum reflectivity based on thermoreflectance is 20 ps, earlier than what is observed experimentally, where the minimum reflectivity is around 60 ps. This difference is likely due to competition between hot carriers, which results in a rise in reflectivity, and heating, which results in a drop in reflectivity, and not necessarily due to an underestimate of the heating time.

Finally, we simulate the process by which the bismuth atoms are driven across the center of the unit cell. This barrier crossing, when combined with strong damping, destroys the Peierls distortion and forms the symmetric phase. To simulate this process, we solve the classical equations of motion numerically for a particle in a time-dependent potential. At every point in time, we use the appropriate lattice potential from the time-dependent carrier density predicted by our extended two-temperature model. This potential surface, along with an empirical damping rate based on the incident fluence [Fig. 2(d)], allows us to solve the equations of motion for the coherent part of the A_{1g} mode trajectory $x(t)$. The equation of motion governing the trajectory of the mode is

$$\mu \frac{\partial^2 x}{\partial t^2} + \Gamma \frac{\partial x}{\partial t} + \frac{\partial V(x,t)}{\partial x} = 0. \quad (6)$$

Here, μ is the effective mass of the A_{1g} mode, and the parameter Γ is the phenomenological damping, which is 0.9 ps^{-1} times the incident fluence in mJ/cm^2, and the potential $V[x, n(t)]$ is the lattice potential given by the time-dependent carrier density $n(t)$ derived from the extended two-temperature model. This scheme is analogous to the equation of motion used in Ref. [5] but with a time-

dependent potential defined by an *ab initio* DFT calculation and a carrier density.

This trajectory can then be converted to a reflectivity change by

$$\frac{\Delta R}{R} = A[x(t)^2 - x_0^2], \tag{7}$$

where x_0 is the initial position of the Bi atom along the *c*-axis direction and $x(t)$ is the time-dependent displacement, where $x = 0$ is the center of the unit cell. The predicted reflectivity change $x(t)^2 - x_0^2$ based on simulated trajectories for incident fluences used in the experiments shown in Fig. 2(a) are shown in Fig. 4(c). The parameter A is a scaling factor that converts displacements to reflectivity through the modulation of the dielectric function. Note that, in the regime the barrier is crossed, we expect strong coupling to other modes [30], strong damping of the A_{1g} mode due to the anharmonicity of the potential, and a loss of Raman activity of the A_{1g} mode [5,10]. The strong damping seen in Fig. 4(c) at high fluences is due to this strongly anharmonic, time-dependent potential, coupled with the velocity damping term in Eq. (6). As the carriers diffuse away from the surface, the barrier in the potential surface reappears. The Peierls distortion does not reappear instantaneously after the barrier reappears, as it takes some time for a macroscopic domain to reform, which accounts for the 2–3 ps delay between the appearance of the coherent phonons in Fig. 3(a) (3–5 ps after excitation) and the carrier density dropping below the switching critical density in Fig. 4(c) (1–3 ps after excitation) [31].

IV. DISCUSSION

Having presented the experimental evidence for the appearance of a high-symmetry crystalline phase of bismuth under strong photoexcitation and thermal modeling that estimates the extent of electronic and thermal excitation near the sample surface, we now return to our picture of the formation of the high-symmetry phase. The key phenomena and timescales are the following, described approximately by the two-temperature model that has been applied to bismuth [21]. Within the excitation pulse duration, the excited electrons equilibrate with each other at the 1.5-eV photon energy, establishing an excited carrier temperature of thousands of degrees Kelvin, which equilibrate with the other valence electrons in tens of femtoseconds [27]. Carriers diffuse out of the 15-nm optical penetration depth of the crystal, while incoherent electron-phonon coupling leads to heating of the lattice, which reaches a maximum temperature in the irradiated region after approximately 25 ps, consistent with optical and electronic spectroscopy measurements [4,24]. The A_{1g} phonon frequency reflects these kinetics. The high initial carrier density leads to a pronounced phonon softening, the extent of which decreases as the excited electrons relax and

diffuse out of the optical penetration depth. The elevated lattice temperature induces a more moderate phonon frequency reduction due to lattice anharmonicity. With moderate pump fluences, such as 6.9 mJ/cm^2, the phonon frequency recovers close to its equilibrium value of 2.9 THz after less than 100 ps, as measured with a second weak pump pulse at long delay times [see Fig. 3(b)]. At higher pump fluences, the phonon frequency does not fully recover even after the longest second-pump delays of 800 ps shown in Fig. 3(b), indicating an elevated lattice temperature that persists for nanoseconds or longer.

In the short time (>150 fs) it takes to form the high-symmetry phase, the unit cell does not have time to change volume, so the primitive lattice likely remains rhombohedral. Within tens of picoseconds following excitation above the threshold for the phase transition, carrier diffusion and thermalization partially restore the lattice potential, which restores lattice ordering along the A_{1g} mode coordinate, resulting in the reappearance of the A_{1g} coherent phonon response after a weak second excitation pulse.

In conclusion, we excited bulk and thin-film bismuth with high fluences, and through the use of a real-time measurement method we observed an ultrafast phase transition into a high-symmetry crystalline phase. Two-pulse measurements show that the symmetric phase in bismuth persists for several picoseconds before the lattice distortion recovers. Our results show that the predicted high-symmetry crystalline phase, which is inaccessible thermally, exists and that it is reached through coherent collective motion of the photoexcited lattice. Direct single-shot observation of coherent motion all the way to far-from-equilibrium structures (despite the photoexcited sample never returning to its pristine state) has enabled a comparison to first-principles theoretical calculations and opens up possibilities for coherent control that could be extended to multidimensional control in materials with complex phase diagrams.

[1] M. Chollet, L. Guerin, N. Uchida, S. Fukaya, H. Shimoda, T. Ishikawa, K. Matsuda, T. Hasegawa, A. Ota, H. Yamochi, G. Saito, R. Tazaki, S.-I. Adachi, and S.-Y. Koshihara, *Gigantic Photoresponse in 1/4-Filled-Band Organic Salt (EDO-TTF)2PF6*, Science **307**, 86 (2005).

[2] S. Iwai, Y. Ishige, S. Tanaka, Y. Okimoto, Y. Tokura, and H. Okamoto, *Coherent Control of Charge and Lattice Dynamics in a Photoinduced Neutral-to-Ionic Transition of a Charge-Transfer Compound*, Phys. Rev. Lett. **96**, 057403 (2006).

[3] É. D. Murray, D. M. Fritz, J. K. Wahlstrand, S. Fahy, and D. A. Reis, *Effect of Lattice Anharmonicity on High-Amplitude Phonon Dynamics in Photoexcited Bismuth*, Phys. Rev. B **72**, 060301 (2005).

[4] D. M. Fritz, D. A. Reis, B. Adams, R. A. Akre, J. Arthur, C. Blome, P. H. Bucksbaum, A. L. Cavalieri, S. Engemann, S. Fahy, R. W. Falcone, P. H. Fuoss, K. J. Gaffney, M. J. George, J. Hajdu, M. P. Hertlein, P. B. Hillyard, M. Horn-von Hoegen, M. Kammler, J. Kaspar *et al.*, *Ultrafast Bond Softening in Bismuth: Mapping a Solid's Interatomic Potential with X-Rays*, Science **315**, 633 (2007).

[5] T. Huber, S. O. Mariager, A. Ferrer, H. Schäfer, J. A. Johnson, S. Grübel, A. Lübcke, L. Huber, T. Kubacka, C. Dornes, C. Laulhe, S. Ravy, G. Ingold, P. Beaud, J. Demsar, and S. L. Johnson, *Coherent Structural Dynamics of a Prototypical Charge-Density-Wave-to-Metal Transition*, Phys. Rev. Lett. **113**, 026401 (2014).

[6] H. Jones, *Applications of the Bloch Theory to the Study of Alloys and of the Properties of Bismuth*, Proc. R. Soc. A **147**, 396 (1934).

[7] S. S. Kabalkina, T. N. Kolobyanina, and L. F. Vereshchagin, *Investigation of the Crystal Structure of the Antimony and Bismuth High Pressure Phases*, Sov. J. Exp. Theor. Phys. **31**, 259 (1970).

[8] H. J. Beister, K. Strössner, and K. Syassen, *Rhombohedral to Simple-Cubic Phase Transition in Arsenic under Pressure*, Phys. Rev. B **41**, 5535 (1990).

[9] B. J. Siwick, J. R. Dwyer, R. E. Jordan, and R. J. Dwayne Miller, *An Atomic-Level View of Melting Using Femtosecond Electron Diffraction*, Science **302**, 1382 (2003).

[10] S. Wall, D. Wegkamp, L. Foglia, K. Appavoo, J. Nag, R. F. Haglund, J. Stähler, and M. Wolf, *Ultrafast Changes in Lattice Symmetry Probed by Coherent Phonons*, Nat. Commun. **3**, 721 (2012).

[11] M. Matsubara, Y. Okimoto, T. Ogasawara, S. Iwai, Y. Tomioka, H. Okamoto, and Y. Tokura, *Photoinduced Switching between Charge and Orbital Ordered Insulator and Ferromagnetic Metal in Perovskite Manganites*, Phys. Rev. B **77**, 094410 (2008).

[12] P. Beaud, A. Caviezel, S. O. Mariager, L. Rettig, G. Ingold, C. Dornes, S.-W. Huang, J. A. Johnson, M. Radovic, T. Huber, T. Kubacka, A. Ferrer, H. T. Lemke, M. Chollet, D. Zhu, J. M. Glownia, M. Sikorski, A. Robert, H. Wadati, M. Nakamura *et al.*, *A Time-Dependent Order Parameter for Ultrafast Photoinduced Phase Transitions*, Nat. Mater. **13**, 923 (2014).

[13] P. Beaud, S. L. Johnson, E. Vorobeva, U. Staub, R. a De Souza, C. J. Milne, Q. X. Jia, and G. Ingold, *Ultrafast Structural Phase Transition Driven by Photoinduced Melting of Charge and Orbital Order*, Phys. Rev. Lett. **103**, 155702 (2009).

[14] L. Stojchevska, I. Vaskivskyi, T. Mertelj, P. Kusar, D. Svetin, S. Brazovskii, and D. Mihailovic, *Ultrafast Switching to a Stable Hidden Quantum State in an Electronic Crystal*, Science **344**, 177 (2014).

[15] E. S. Zijlstra, N. Huntemann, and M. E. Garcia, *Laser-Induced Solid-Solid Phase Transition in As under Pressure: A Theoretical Prediction*, New J. Phys. **10**, 033010 (2008).

[16] B. Bauerhenne, S. Krylow, M. E. Garcia, E. S. Zijlstra, and T. Zier, *Ab Initio Molecular Dynamics Simulations of Femtosecond-Laser-Induced Anti-Peierls Transition in Antimony*, Proc. SPIE **9735**, 97350K (2016).

[17] G. Sciaini, M. Harb, S. G. Kruglik, T. Payer, C. T. Hebeisen, F.-J. Meyer zu Heringdorf, M. Yamaguchi, M. Horn-von Hoegen, R. Ernstorfer, and R. J. Dwayne Miller, *Electronic Acceleration of Atomic Motions and Disordering in Bismuth*, Nature (London) **458**, 56 (2009).

[18] K. Sokolowski-Tinten, C. Blome, J. Blums, A. Cavalleri, C. Dietrich, A. Tarasevitch, I. Uschmann, E. Förster, M. Kammler, M. Horn-von Hoegen, and D. von der Linde, *Femtosecond X-Ray Measurement of Coherent Lattice Vibrations near the Lindemann Stability Limit*, Nature (London) **422**, 287 (2003).

[19] T. Shin, J. W. Wolfson, S. W. Teitelbaum, M. Kandyla, and K. A. Nelson, *Dual Echelon Femtosecond Single-Shot Spectroscopy*, Rev. Sci. Instrum. **85**, 083115 (2014).

[20] See Supplemental Material at http://link.aps.org/supplemental/10.1103/PhysRevX.8.031081 for film characterization, conventional pump-probe measurements, additional information about the single-shot method, laser-induced damage characterization, and additional details of the extended two-temperature model.

[21] T. Shin, S. W. Teitelbaum, J. Wolfson, M. Kandyla, and K. A. Nelson, *Extended Two-Temperature Model for Ultrafast Thermal Response of Band Gap Materials upon Impulsive Optical Excitation*, J. Chem. Phys. **143**, 194705 (2015).

[22] T. Shin, J. W. Wolfson, S. W. Teitelbaum, M. Kandyla, and K. A. Nelson, *Carrier Confinement and Bond Softening in Photoexcited Bismuth Films*, Phys. Rev. B **92**, 184302 (2015).

[23] T. Garl, E. G. Gamaly, D. Boschetto, A. V. Rode, B. Luther-Davies, and A. Rousse, *Birth and Decay of Coherent Optical Phonons in Femtosecond-Laser-Excited Bismuth*, Phys. Rev. B **78**, 134302 (2008).

[24] C. M. Liebig, Y. Wang, and X. Xu, *Controlling Phase Change through Ultrafast Excitation of Coherent Phonons*, Opt. Express **18**, 20498 (2010).

[25] A. Q. Wu and X. Xu, *Coupling of Ultrafast Laser Energy to Coherent Phonons in Bismuth*, Appl. Phys. Lett. **90**, 251111 (2007).

[26] B. Arnaud and Y. Giret, *Electron Cooling and Debye-Waller Effect in Photoexcited Bismuth*, Phys. Rev. Lett. **110**, 016405 (2013).

[27] Y. Giret, A. Gellé, and B. Arnaud, *Entropy Driven Atomic Motion in Laser-Excited Bismuth*, Phys. Rev. Lett. **106**, 155503 (2011).

[28] K. Sokolowski-Tinten, in *Proceedings of the International Conference on Ultrafast Phenomena* (Optical Society of America, Washington, D.C., 2016), p. UTh4A.49.

[29] B. Rethfeld, K. Sokolowski-Tinten, D. von der Linde, and S. I. Anisimov, *Ultrafast Thermal Melting of Laser-Excited Solids by Homogeneous Nucleation*, Phys. Rev. B **65,** 092103 (2002).

[30] E. S. Zijlstra, L. L. Tatarinova, and M. E. Garcia, *Laser-Induced Phonon-Phonon Interactions in Bismuth*, Phys. Rev. B **74,** 220301 (2006).

[31] R. Yusupov, T. Mertelj, V. V. Kabanov, S. Brazovskii, P. Kusar, J.-H. Chu, I. R. Fisher, and D. Mihailovic, *Coherent Dynamics of Macroscopic Electronic Order through a Symmetry Breaking Transition*, Nat. Phys. **6,** 681 (2010).